Journal of Non-Crystalline Solids 358 (2012) 1740–1745

Contents lists available at SciVerse ScienceDirect

Journal of Non-Crystalline Solids

journal homepage: www.elsevier.com/ locate/ jnoncrysol

Evolution of glass properties during a substitution of S by Se in $Ge_{28}Sb_{12}S_{60-x}Se_x$ glass network

Guillaume Guery [a,b,*], J. David Musgraves [a], Christine Labrugere [b], Evelyne Fargin [b], Thierry Cardinal [b], Kathleen Richardson [a]

[a] School of Materials Science and Engineering, COMSET, Clemson University, Clemson, SC 29634, USA
[b] Institut de Chimie de la Matière Condensée de Bordeaux (ICMCB-CNRS) UPR 9048, Université de Bordeaux I, Avenue du Dr Schweitzer, 33608 Pessac Cedex, France

ARTICLE INFO

Article history:
Received 7 February 2012
Received in revised form 27 April 2012
Available online 9 June 2012

Keywords:
Chalcogenide glass;
Raman spectroscopy;
X-ray photoelectron spectroscopy;
Glass properties

ABSTRACT

In this paper, a detailed study to examine the influence of chalcogen S/Se mole % in the $Ge_{28}Sb_{12}S_{60-x}Se_x$ glass system, with $x=0$, 15, 30, 45 and 60, is presented that provides insight into the effect of chalcogen content on the glass network and properties. Specifically, we report results of a systematic study to evaluate the relationship between compositional variation, glass properties and dominant bonding configurations. These materials are important to applications in optics manufacturing where correlation of physical and optical properties is required to predict fabrication behavior and ultimate material performance. It has been found that the dominant bonds in the glass system change upon reaching a specific molar ratio (percentage, %) of chalcogen substitution, between $30<x<45$ mol%, changing from Ge—Se to Sb—Se bonds as the dominant bond type. This singularity has been observed using micro-Raman spectroscopy and X-ray photoelectron spectroscopy. This effect of the dominant bond configurational change was also shown to impart changes in important physical properties including micro-hardness, thermal properties, and the glass' viscometric behavior. Results indicate that the observed dominant bond change was responsible for a constant value in the evolution of both the micro-hardness and calorimetric glass transition temperature. The viscosity was also affected by the change in dominant bond type, breaking the monotony of the viscosity evolution during the S substitution, due to the total strength of the vitreous system which does not linearly increase.

1. Introduction

Chalcogenide glasses (ChGs) have attracted the attention of many investigators due to the fact that they are used in applications for infrared optics, reversible optical recording, photonic devices, memory switching [1,2] and more recently, in precision glass molding (PGM) [3]. Additionally, selenide and sulfide-containing ChG materials have been identified as possible materials for nonlinear optical applications. Several investigations [4-8] have evaluated the difference in physical and optical properties between both chalcogen systems (based solely on sulfur or selenium), but these works have not systematically investigated the influence of S substitution for Se on the structure and glass properties yet.

Prior efforts from Richardson et al. Frumar et al., Giridhar et al., Narasimham et al. have widely investigated GeSbS glasses and the influence of Se for S substitution on the linear and nonlinear optical properties of the material. These compositions were largely in the $Ge_{23}Sb_7S_xSe_{70-x}$ (written here as 23-7-70) composition space, which is lower in Ge content than commercially available $Ge_{28}Sb_{12}Se_{60}$ compositions manufactured by Schott Glass and Amorphous Materials under the trade names IG-5 and AMTIR-3. These latter glasses (IGs and AMTIR compositions) are widely used in commercial optical systems and thus, are of importance to optical designers interested in fabricating precision optical components via conventional (grinding and polishing) or more advanced (precision glass molding, PGM) methods [9]. Thus, as optical properties (transmission, refractive index and dispersion) and thermo-mechanical attributes (viscosity, hardness and structural relaxation behavior) of these materials have been shown to vary with chalcogen type, the current study aims to evaluate how S/Se ratio impacted properties important to optical design and manufacturing efforts.

This paper examines glasses in the Ge—Sb—S—Se system with high crystallization stability, $\Delta T>100°$ (defined as T_x-T_g), and has systematically evaluated physical property changes in the glass associated with a substitution of Se for S in the amorphous network. Glasses in the amorphous system $Ge_{28}Sb_{12}S_{60-x}Se_x$ with $x=0$, 15, 30, 45 and 60 have been investigated and the resulting variation in physical properties quantified. Raman spectroscopy and X-ray photoelectron spectroscopy (XPS) have been used to evaluate the modifications in glass structure as S is progressively replaced by Se. A correlation is established between molecular units in the glass network and the corresponding fluctuation of glass properties. The

* Corresponding author at: School of Materials Science and Engineering, COMSET, Clemson University, Clemson, SC 29634, USA. Tel.: +1 8646561259.
E-mail address: gguery@clemson.edu (G. Guery).

0022-3093/$ – see front matter © 2012 Elsevier B.V. All rights reserved.
doi:10.1016/j.jnoncrysol.2012.05.007

impact of these structural changes on mechanical (micro-hardness) and thermal (viscosity) behavior has also been quantified.

2. Experimental procedures

2.1. Sample preparation

Sulfide glasses in the vitreous system $Ge_{28}Sb_{12}S_{60-x}Se_x$ with $x=0$, 15, 30, 45 and 60 were examined in this study and were prepared in 10 g batches. The glasses were prepared from high purity elements (Ge 99.999% (Alfa Aesar), Sb 99.999% (Sigma-Aldrich), S 99.998% (Aldrich), Se 99.999% (Alfa Aesar)). The starting materials were weighed and batched inside a nitrogen-purged glove box and sealed using a gas–oxygen torch under vacuum into quartz ampoules. The ampoule was then heated for 16 h at between 875 and 925 °C, depending on the glass composition. A rocking furnace was used to rock the ampoule during the melting to increase the homogeneity of the melt. Once homogenized, the melt-containing ampoule was air-quenched to room temperature. To avoid fracture of the tube and glass ingot, the glasses were subsequently returned to the furnace for annealing for 15 h at 40 °C below the respective glass transition temperature, T_g, of the glass. The sulfo-selenide glass samples were then cut, optically polished, and inspected visually.

Glass compositions were verified by energy-dispersive X-ray spectroscopy (EDS) and were found to be identical to the initial concentrations introduced in the batch. No loss of sulfur was observed within the accuracy of the measurement (±2%). X-ray diffraction was carried out on each sample to confirm the amorphous state of the investigated samples.

2.2. Property measurements

Raman spectra were obtained using a Senterra (Bruker Optik) micro Raman system using a 785 nm excitation wavelength with a laser power level of 1 mW. The use of this near-infrared (NIR) radiation for Raman excitation was specific to our study, in that excitation was at an energy and power level well below the band gap region for these samples, thus eliminating the possibility of inducing photo-structural modification in the glass from the probe beam during measurements. Confirmation that this analysis did not change the glass structure was obtained by repeating the analysis on the same spot twice in a row for each measurement.

XPS data were collected using a VG Scientific 220i-XL ESCALAB system. The non-monochromatized MgKα X-ray source (1253.6 eV) was used to acquire the surveys at 150 eV of constant pass energy and the high-resolution spectra at 20 eV. Binding energies were referenced to the C (1 s) energy at 284.7 eV. Experimental peaks were fitted using Gaussian–Lorentzian mixtures with the "AVANTAGE" software provided by ThermoFisher Scientific. Freshly fractured surfaces were analysed after cleaving the glasses and introducing them immediately into vacuum. The residual pressure in the analysis chamber was in the 10^{-7} Pa range.

In this study, a Shimadzu DUH-211 S Micro-hardness tester was used, with a Vickers diamond indenter with a square base and an angle of 136 degrees between opposite faces. A static load of 2000 mN made with a loading rate of 13.3240 mN/min, generating indentations with no residual lateral cracking was used for the experiments; the reported micro-hardness values represent the average of fifteen tests. The diagonal length of indentation was measured after the test and the micro-hardness was then calculated.

The glass transition temperatures (T_g), the onset of the crystallization peak (T_x) and the crystallization temperature (T_p) were determined by Differential Scanning Calorimetry (DSC) at a heating rate of 10 °C/min from 50 to 550 °C using a commercial DSC apparatus (DSC 2920, TA instruments). The instrumental error of all measured values is ±2 °C. The measurements were carried out in hermetically sealed aluminium pans. The glass transition temperature (T_g) was taken as the inflection point of the endotherm (obtained by taking the first derivative of the curve), and the crystallization temperature (T_p) at the maximum of the exothermic peak. Crystallization stability, $\Delta T = T_x - T_g$, was calculated to confirm the vitreous nature of the glasses ($\Delta T > 100$ °C) within the temperature ranges examined, permitting glasses to be crystal-free, and maximizing the IR transparency of the specimens.

The glass viscosity properties in the softening region (across the range of Log $\eta = 3.0$–6.0 Pa s) were measured with a PPV-1000 parallel-plate viscometer from Orton Ceramics. As the sample height changes as a function of time and temperature, a LVDT (Linear Variable Differential Transformer) coil, residing on the compensation arm and attached to the adjacent sample arm, monitors the magnitude and direction of the initial specimen's (4 mm high) height change. The compensation arm is attached via a hollow, fused quartz support rod to an Inconel® compensation block (12 mm thickness), which houses the sample temperature thermocouple. By attaching the LVDT to an Inconel® compensation block, system movement and Inconel® plate expansion are nullified from the LVDT signal. The insulation acts as the top of the furnace in the raised position for experimental measurements. The 1000 °C, Kanthal wound, ceramic fiber-lined furnace can be raised and lowered with a motor to house the glass sample.

3. Results

The purpose of this study was to investigate the effect of the substitution of S for Se on the glass network in the GeSb-based glasses. Raman spectroscopy and X-ray photoelectric spectroscopy (XPS) have been used to track these structural evolutions during the chalcogen specie substitution. Discussion will be focused on the evolution of the bands in the Raman spectra, related to the evolution of features within the XPS spectra.

The Raman spectra of the investigated glasses are shown below in Fig. 1.

The spectrum of the sulphide glass ($x=0$) in the Ge–Sb system exhibits 4 broad bands with the maximum intensity peaking at around 160, 210, 260 and 330 cm^{-1}. A vibration at 150 cm^{-1} is assigned to the F_2 mode of $GeS_{4/2}$ groups [10]. Vibrations between 210 and 260 cm^{-1} have been attributed to the molecular entities containing fewer than 4 sulfur atoms around Ge centers (the glass is sulfur deficient), and vibrations related to homopolar bonds are clearly observed. A vibration related to the presence of Sb-Sb linkages has been reported at 163 cm^{-1} [11], while the band at 260 cm^{-1} is associated by Luvosky et al. to the stretching of Ge–Ge homopolar bonds in the S_3Ge–GeS_3 units [12]. The main band around 342 cm^{-1} has been assigned by Sugai et al. to the A_1 symmetric stretching vibration of S atoms in GeS_4 units. The vibration around 375 cm^{-1}, called the companion A_1^C band, is attributed to edge sharing tetrahedral sites [13]. According to Jackson et al. and also reported by Petit et al., the weak band located around 400 cm^{-1} may arise from the T_2 mode of corner-sharing GeS_4 units[7]. Bands at 287 and 308 cm^{-1} have been attributed by Frumarova et al. to E and A_1 modes of SbS_3 units respectively [14].

The spectrum of the sulfur-free selenide glass ($x=60$) in the Ge–Sb system exhibits three broad bands located around 160, 200 and 260 cm^{-1}. The first broad band at around 160 cm^{-1}, contains what are believed to be two convolved peaks. Vibrations at 152 cm^{-1} correspond to the homopolar bond Sb–Sb in the Se_2Sb–$SbSe_2$ molecular unit [11,15]. The vibration at 174 cm^{-1} is attributed to $Ge_2Se_{6/2}$ [16]. Regarding the second broad band at around 200 cm^{-1}, three contributions have been reported. The vibration at 192 cm^{-1} represents the Sb–Se linkage in $SbSe_{3/2}$ pyramids [17]. In accordance with Lucovsky and al., the band at 200 cm^{-1} has been assigned to the ν_1 mode of corner-sharing of $GeSe_{4/2}$ [12,18,19]. The frequency at 215 cm^{-1} is

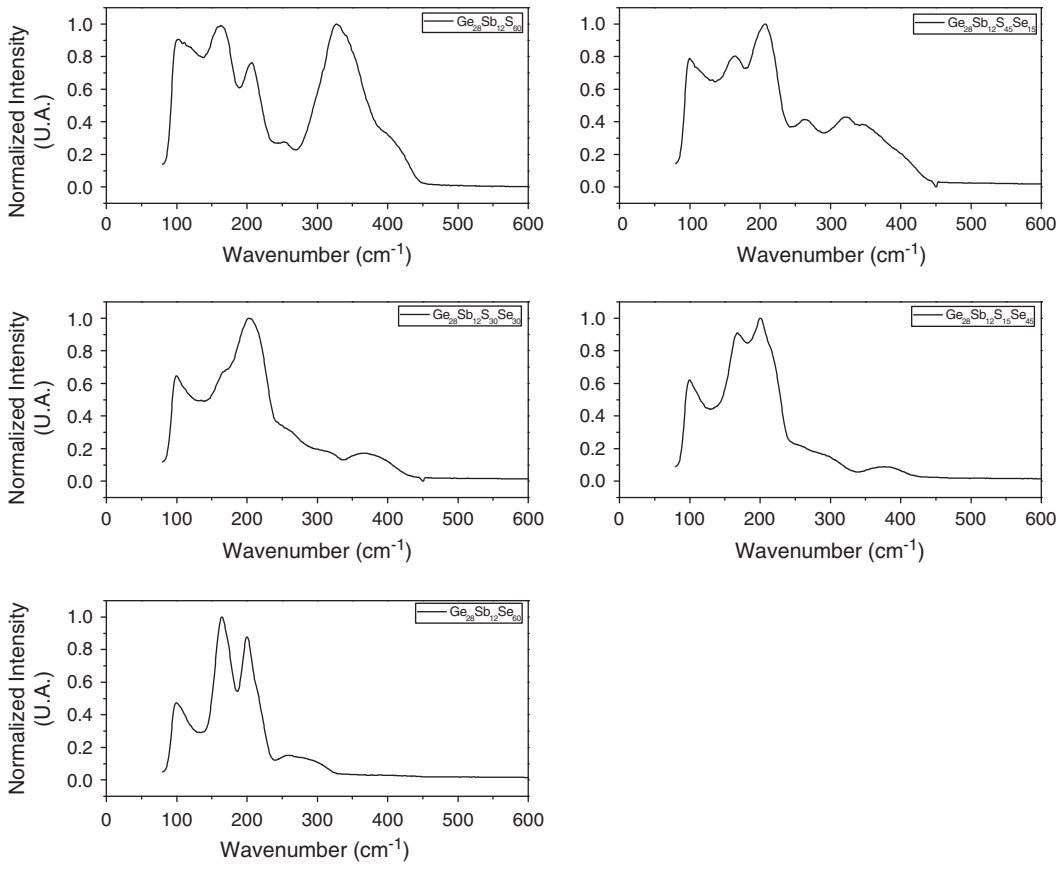

Fig. 1. Raman spectra of $Ge_{28}Sb_{12}S_{60-x}Se_x$ versus *x*.

correlated to A^C_1 breathing vibration of edge-sharing of $Ge_2Se_{8/2}$ [7]. The vibration at 260 cm^{-1} is linked to the F_2 vibration of $GeSe_{4/2}$ molecular units [18,19]. The vibration located at 280 cm^{-1} is related to the electronic density of germanium [20]. The frequency at 300 cm^{-1} is associated to F_2 asymmetric vibration modes of $GeSe_4$ tetrahedra [17].

When sulfur is replaced by selenium, namely *x* (% Se) increases, the relative intensity of the bands associated with sulfur, located between 275 cm^{-1} and 450 cm^{-1} progressively decrease and new bands appear below 230 cm^{-1}. Two main bands at 152 and 192 cm^{-1} emerge, respectively attributed to the homopolar bond Sb-Sb in the $Se_2Sb–SbSe_2$ molecular unit, and to Sb–Se linkage in $SbSe_{3/2}$ pyramids. Above $x=15$, the intensity of the broad band at 200 cm^{-1} increases, and at $x=45$, two contributions are clearly seen at around 200 cm^{-1} and 215 cm^{-1}. These bands may be related to the Sb-Se linkage in $SbSe_{3/2}$ pyramids proposed by Petit et al. at 192 cm^{-1}, to the ν_1 mode of corner-sharing of $GeSe_{4/2}$ proposed by Lucovsky et al. at 200 cm^{-1} [12], and thus to A^C_1 breathing vibration of edge-sharing of $Ge_2Se_{8/2}$ also proposed by Petit et al. at 215 cm^{-1} [7].

The XPS Sb spectrum in $Ge_{28}Sb_{12}S_{60-x}Se_x$ (with $x=0$, 30 and 60) is represented by a main double peak corresponding to $Sb3d_{5/2}$ and $Sb3d_{3/2}$ The studied system presents complex spectra due to overlaps of peaks (i.e. $Sb3d_{5/2}$ with O1s, Se3p with S2p, Sb4d with Ge3d). The most important result is the shift of the peak to lower energy as the sulfur is replaced for selenium. Indeed, we can observe in Fig. 2, a shift of the peaks during the substitution from 529.3–528.3 eV (for $x=0$) to 528.6–527.4 eV (for $x=60$). The presence of the oxygen contribution is due to oxygen contamination during the batch preparation or during the fresh fracture.

The XPS Ge3d–Sb4d5/Sb4d3 spectrum consists of two bands described by a single Gaussian contribution for Ge3d around 32 eV and by two Gaussians for Sb4d5 and Sb4d3 around 34–35 eV, as shown in Fig. 3. According to the average coordination number $<r>=2.68$ as defined by Phillips et al. [21], taking into account that the coordination numbers of Ge, Sb and S is respectively 4, 3 and 2, in agreement with previous investigation mainly Sb^{3+} species are expected in the glass matrix as discussed by Jiang et al. for sulfide [22].

In the bulk sulfide glass ($x=0$), the peak related to Ge3d is more intense than those for Sb4d5/Sb4d3, whereas during the substitution ($x=30$), this tendency changes. Finally in the selenide glass ($x=60$), the peak assigned to Sb4d5 is the most intense in the spectrum. Furthermore, the Ge3d peak becomes narrower, with a full width at half maximum (FWHM) changing from 2.17 eV to 1.83 eV.

The Vickers micro-hardness of the investigated glasses is shown below in Fig. 4 for the glasses examined. In this glass system, a decrease of the hardness is clearly observed when sulfur is substituted for selenium. This can be explained by the average bond strengths present in the glass ($E_{Ge\text{-}Se}=230$ kJ/mol, $E_{Ge\text{-}S}=279$ kJ/mol, $E_{Sb\text{-}Se}=225$ kJ/mol, $E_{Sb\text{-}S}=205$ kJ/mol, [22,23]), which are higher in the sulfide glasses than in the selenide glass. Similar results were obtained previously in related compositions [7].

Table 1 summarizes the variation in glass transition temperature (T_g), temperature of crystallization onset (T_x), crystallization temperature (T_p) and the crystallization stability ($\Delta T=T_x-T_g$) with chalcogen type and ratio. T_g and T_x decrease during the substitution of S for Se due to a difference in the bond strengths as noted above. As shown in Fig. 5, T_g decreases during the substitution with a constant value at 30–45 mol%. Furthermore, all compositions have a $\Delta T>100$ °C, which means that glasses have excellent stability against crystallization and no evidence of crystallization was noted in any glasses prepared or measured in this study.

Viscosity of the investigated glasses has been measured between Log $\eta=3.0$–6.0 Pa.s using a parallel plate viscometer (PPV) and the data are shown below in Fig. 6a. The system isokom, indicating the temperatures at which each glass has a viscosity of 10^5 Pa.s is

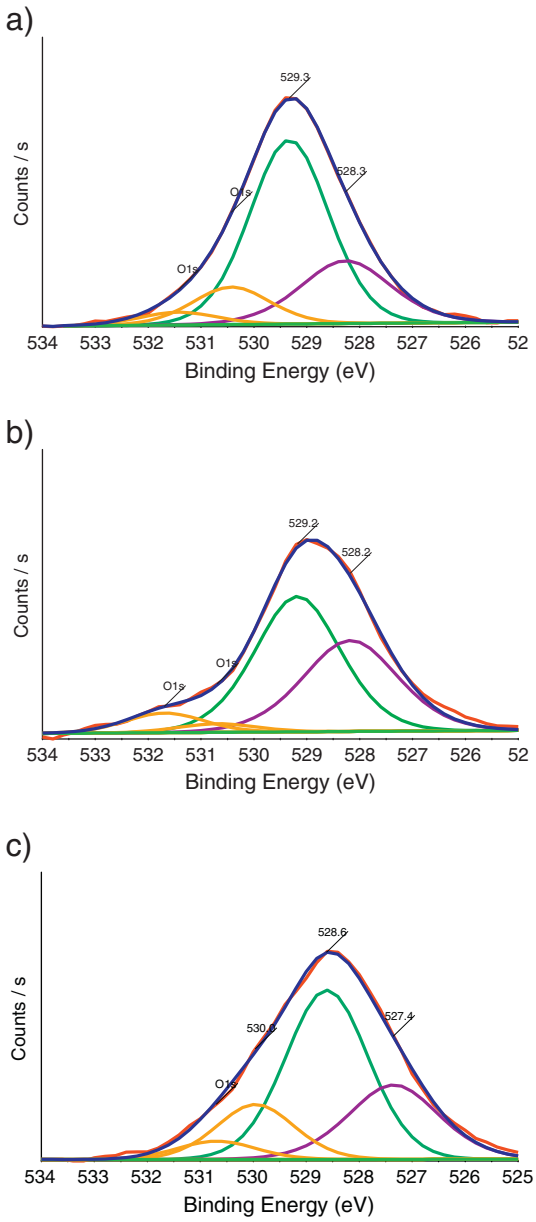

Fig. 2. High resolution XPS spectrum of $Sb3d_{5/2}$ levels for the investigated a) $Ge_{28}Sb_{12}S_{60}$, b) $Ge_{28}Sb_{12}S_{30}Se_{30}$ and c) $Ge_{28}Sb_{12}Se_{60}$.

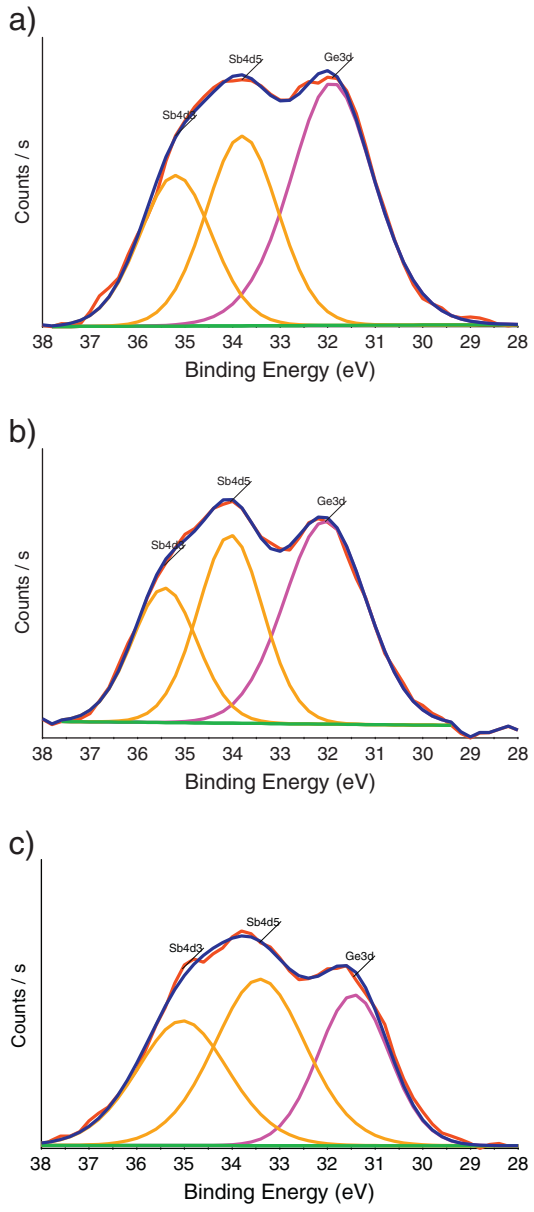

Fig. 3. High resolution XPS spectrum of Ge3d levels for the investigated a) $Ge_{28}Sb_{12}S_{60}$, b) $Ge_{28}Sb_{12}S_{30}Se_{30}$ and c) $Ge_{28}Sb_{12}Se_{60}$.

shown in Fig. 6b. This viscosity region represents the *working region*, where the glass is soft enough to be manipulated for obtaining different shapes (e.g. fiber, aspherical lens).

Trends in the data points from the PPV measurements indicate that when sulfur is substituted by selenium, the log (viscosity) curve shifts to a lower temperature.

4. Discussion

The aim of this study was to investigate the effect Se substitution for S on the glass structure and physical properties in Ge–Sb-based sulphide glasses. Raman spectroscopy and X-ray photoelectron spectroscopy were used to evaluate and track the structural modification through systematic substitution of Se atom for S. This discussion will be focused on the evolution of the Raman bands, their features and the relative fraction of various species in the glass network, and will be linked to changes in relevant structure-sensitive thermal and physical properties.

The $Ge_{28}Sb_{12}S_{60-x}Se_x$ glass system is not a stoechiometric composition. Indeed, in a stoichiometric composition, Sb_2S_3 and GeS_2 are the primary molecular units and there are no homopolar bonds present. In the present case, all glasses examined are deficient in sulfur (chalcogen) meaning that homopolar bonding of the non-chalcogen species can be expected. Homopolar bonds such as Ge—Ge and Sb—Sb can be assumed to be present, in this case.

As noted ealier, the Raman band at 342 cm^{-1} decreases whereas the bands at 152 and 192 cm^{-1} increase during the substitution of sulfur for selenium. This evolution indicates that the fraction of GeS_4 molecular units, which are dominant in the sulfur-rich end of the glass system, decreases and are replaced by Sb-based bonds such as the homopolar Sb—Sb bond and $SbSe_{3/2}$ pyramidal units.

X-ray photoelectronic spectroscopy measurements have been performed in order to corroborate the evolution of the glass network suggested by the Raman spectra. Changes of peak intensity seen in Raman spectra, which translate to switch of dominant bonds present in the glass network, is here studied by XPS, showing the evolution of the atomic fraction of each component present in the vitreous system.

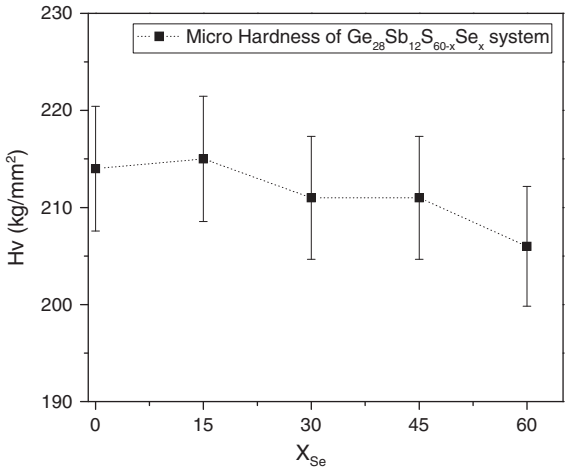

Fig. 4. Evolution of the micro-hardness as function of the substitution of S by Se in $Ge_{28}Sb_{12}S_{60-x}Se_x$ glass system. Static load equals 10 mN. Errors bars shown are ±3%.

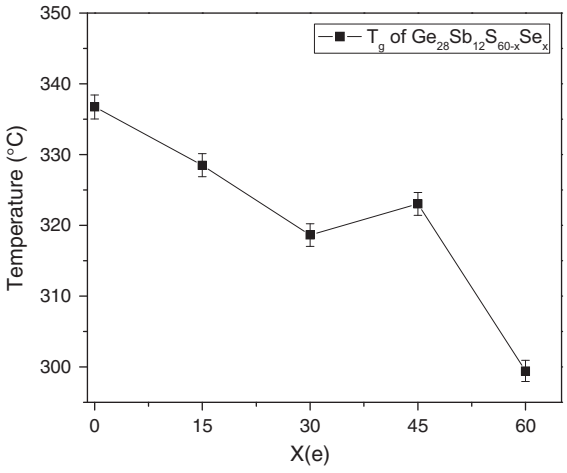

Fig. 5. Evolution of the glass transition temperature T_g as function of the substitution of S by Se in glass system.

Focusing on the 530–540 eV range shown in Fig. 2, we can observe that the peaks assigned to Sb3d5/2 shift in energy during the chalcogen substitution from 529.3–528.3 eV to 528.6–527.3 eV. This shift is due to the change of cation linked to the Sb atoms, i.e. Sb—S to Sb—Se. The 30–40 eV range examined in Fig. 3 shows that the intensity ratio Ge3d to Sb4d5 features has changed. Indeed, during the chalcogen substitution, the highest peak intensity shifts from the Ge3d (for $x=0$) to the Sb4d5 (for $x=60$) feature. The significance of these changes is related to the contribution of each species, indicating a change in the dominant bond type in the glass network [24,25]. Regarding the germanium contribution, based on the width and the area of its peak, we can observe that the FWHM decreases from 2.17 eV to 1.83 eV. Such an evolution is indicative of a narrower distribution of sites for the germanium centers. In the selenium glass ($x=60$) the site distribution around germanium is the narrowest. The increase of the selenium content tends to limit the distribution of sites for germanium centers and increase the variety of antimony sites. Such a hypothesis is in accordance with the appearance in the Raman spectra of significant Sb—Sb vibration contribution for selenium rich samples, which were not evident in the sulfur rich glass.

This change of dominant bond type in the glass network is at the origin of the glass property modifications exhibited by this family. As shown in Fig. 4, the physical properties (i.e. microhardness) are only modestly changed. The micro-hardness slowly decreases during the S substitution, but it can be seen that in the $x=30$–45 region, a flat evolution appears which reflects a non-linear evolution in the total bond strength in the vitreous system; because the ratio of the different species ($GeS_{4/2}$ to $SbSe_{3/2}$) is not linear with the S substitution, the total bond strength, reflected in the hardness, is not linear.

Thermal properties are also dependent on the nature of the dominant bonds present in the glass network. Fig. 5 shows the evolution of the glass transition temperature of the system as function of the atomic percent of Se in the glass. Here we can observe that T_g does not decrease monotonically across the composition space. A constant value is present in the $x=30$–45 region, which again reflects a change in dominant bonds in the network; indeed, as T_g represents onset of mobility in the network this temperature is dominated by the majority network structure.

Note again that glasses at x=30 and 45 exhibit similar viscosity behavior, shown in Fig. 6a, and more explicitly in Fig. 6b, indicating

Table 1
Table of characteristic temperature in $Ge_{28}Sb_{12}S_{60-x}Se_x$ glass system. Error bars shown are ±2 °C.

Composition	T_g (°C)	T_x (°C)	T_p (°C)	$\Delta T=T_x-T_g$
$Ge_{28}Sb_{12}S_{60}$	342	526	544	184
$Ge_{28}Sb_{12}S_{45}Se_{15}$	323	511	–	188
$Ge_{28}Sb_{12}S_{30}Se_{30}$	319	493	–	174
$Ge_{28}Sb_{12}S_{15}Se_{45}$	322	496	460	174
$Ge_{28}Sb_{12}Se_{60}$	297	491	392	194

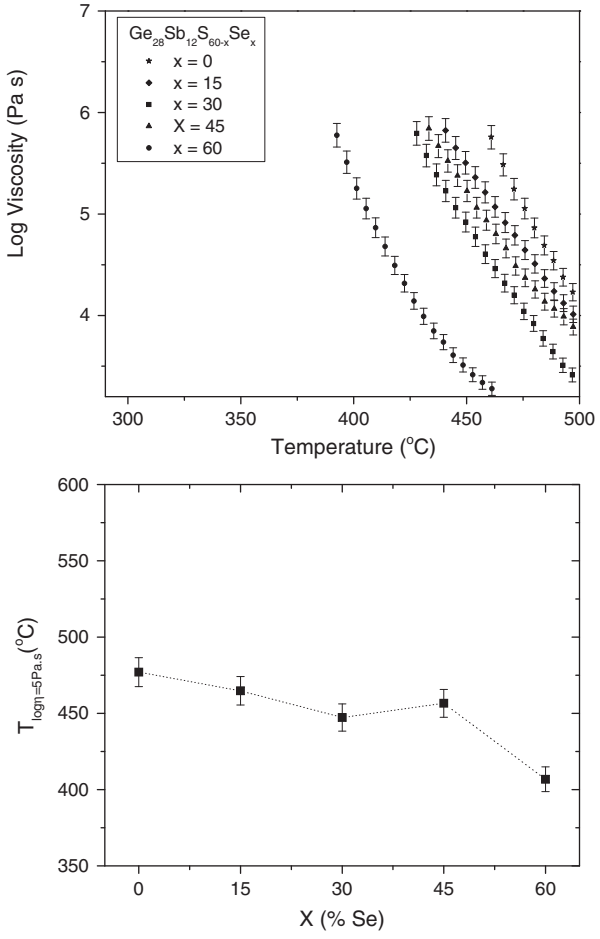

Fig. 6. a) Evolution of the transition range viscosity behavior in the $Ge_{28}Sb_{12}S_{60-x}Se_x$ glass system as a function of Se content (x, mol%). b) Evolution of the drawing temperature of $Ge_{28}Sb_{12}S_{60-x}Se_x$ glass system as function of Se content (x, mol%).

the evolution of the specific drawing temperature. This trend is expected, considering again that the strength of the Se bonds is lower than that of the S bonds, and thus require less thermal energy to cause weakening of the glass network and the onset of flow. As soon as the sulfur is present ($x = 45$), the material properties tends to the pure sulfide making a significant break with the behavior of the pure selenide.

5. Conclusion

In this paper, we have shown that the progressive introduction of Se for S in germanium-antimony based-sulfide glasses does not follow a linear trend of the relative fraction of various species in term of thermal and mechanical properties. Raman spectroscopy and X-ray photoelectron spectroscopy provided evidence of a clear change of dominant bonds in the chalcogenide glass network, upon substitution of S by Se. This change of dominant bond was correlated to variations in glass properties: decreasing micro-hardness and glass transition temperature with, each time, the same value in $x = 30$–45 region. This observation was also seen into the evolution of the viscosity. We observed that viscosities of $Ge_{28}Sb_{12}S_{30}Se_{30}$ and $Ge_{28}Sb_{12}S_{15}Se_{45}$ glasses were switched, due to this change of the dominant bonds. A gap in term of thermal and mechanical properties is observed between the $Ge_{28}Sb_{12}S_{15}Se_{45}$ and $Ge_{28}Sb_{12}Se_{60}$ compositions which is related to the formation of different antimony sites and significant formation of Sb—Sb bonds.

References

[1] Z. Ling, H. Ling, Z. Cheng Shan, J. Non-Cryst. Solids 184 (1995) 1.
[2] A. Znobrik, J. Stetzif, I. Kavich, V. Osipenko, I. Zachko, N. Balota, O. Jakivchuk, Ukr. Phys. J. 26 (1981) 212.
[3] E. Guillevic, X. Zhang, T. Pain, L. Calvez, J.L. Adam, J. Lucas, M. Guilloux-Viry, S. Ollivier, G. Gadret, Opt. Mater. 31 (2009) 1688–1692.
[4] A. Giridhar, J. Non-Cryst. Solids 43 (1981) 29–35.
[5] P.S.L. Narasimham, J. Non-Cryst. Solids 43 (1981) 301–305.
[6] S. Mahadevan, J. Non-Cryst. Solids 57 (1983) 423–430.
[7] L. Petit, N. Carlie, K. Richardson, Y. Guo, A. Schulte, B. Campbell, B. Ferreira, S. Martin, J. Phys. Chem. Solids 66 (2005) 1788–1794.
[8] L. Petit, Mater. Res. Bull. 42 (2007) 2107–2116.
[9] B. Gleason, P. Mosaddegh, P. Wachtel, J.D. Musgraves, K. Richardson, An introduction to the Dyna Technologies Inc. precision molding machine, SPIE Optifab. Rochester, New York, 2011 May 9-13.
[10] E.I. Kamitsos, J.A. Kapoutsis, G.D. Chryssikos, G. Taillades, A. Pradel, M. Ribe, J. Solid State Chem. 112 (2) (1994) 255–261.
[11] I. Watanabe, S. Noguchi, T. Shimizu, J. Non-Cryst. Solids 58 (1983) 35.
[12] G. Lucovsky, F.L. Galeener, R.C. Keezer, R.H. Geils, H.A. Six, Phys. Rev. B 10 (1974) 5134–5146.
[13] S. Sugai, Phys. Rev. B 35 (1987) 1345.
[14] B. Frumarova, J. Non-Cryst. Solids 256–257 (1999) 266–270.
[15] Z.G. Ivanova, E. Cernoskova, V.S. Vassilev, S.V. Boycheva, Mater. Lett. 57 (2003) 1025.
[16] P. Nemec, B. Frumarova, M. Frumar, J. Non-Cryst. Solids 270 (2000) 137.
[17] L. Petit, N. Carlie, R. Villeneuve, J. Massera, M. Couzi, A. Humeau, G. Boudebs, K. Richardson, J. Non-Cryst. Solids 352 (2006) 5413–5420.
[18] D.R. Goyal, A.S. Maan, J. Non-Cryst. Solids 183 (1995) 182–185.
[19] S.M. El-Sayed, Semicond. Sci. Technol. 18 (2003) 337–341.
[20] Z. Boqiang, J. Non-Cryst. Solids 95–96 (1987) 295–302.
[21] J.C. Phillips, J. Non-Cryst. Solids 34 (2) (1979) 153–181.
[22] L. Jiang, A.G. Fitzgerald, M.J. Rose, K. Christovaa, A. Manova, V. Pamukchievaa, J. Optoelectron. Adv. Mater. 3 (3) (2001) 841–846.
[23] E.V. Shkol'nikov, Sov. J. Glass Phys. Chem. 11 (1985) 40.
[24] L. Petit, Phys. Chem. Glasses 45 (6) (2004) 315–321.
[25] T. Ueno, J. Appl. Phys. 21 (1982) 230.